Robust Kernel Estimation with Outliers Handling for Image Deblurring Supplemental Material

Jinshan Pan[1,2], Zhouchen Lin[3,4,*], Zhixun Su[1], Ming-Hsuan Yang[2]
[1]School of Mathematical Sciences, Dalian University of Technology
[2]Electrical Engineering and Computer Science, University of California at Merced
[3]Key Laboratory of Machine Perception (MOE), School of EECS, Peking University
[4]Cooperative Medianet Innovation Center, Shanghai Jiaotong University
sdluran@gmail.com, zlin@pku.edu.cn, zxsu@dlut.edu.cn, mhyang@ucmerced.edu

Overview

In this supplemental material, we analyze the proposed kernel estimation method and demonstrate why it is able to estimate blur kernels from blurred images with outliers in Section 1. We further show that the proposed algorithm can be applied to improve existing methods in Section 2. We quantitatively evaluate the proposed method on the dataset with outliers and images with random noise in Sections 4 and 5, respectively. We further evaluate the proposed method on natural image deblurring datasets [12] and [10], and show that it performs well against the state-of-the-art deblurring methods in Section 6. Section 7 presents some challenging examples with comparisons of state-of-the-art deblurring methods. The implemented code and dataset are available at https://sites.google.com/site/jspanhomepage/

1. Effectiveness of Proposed Method

As mentioned in Section 4.1 of the manuscript, most state-of-the-art deblurring algorithms fail to generate blur kernels when blurred images contain outliers. Thus, we propose an effective outlier detection method to remove outliers from extracted salient edges. Figure 1 shows an example which illustrates how the proposed method generates blur kernels from blurred images with significant outliers.

To further understand the proposed algorithm, we generate a synthetic example as shown in Figure 2(a) and show some intermediate results in Figure 2. The detected outliers are refined over iterations.

Difference from Outlier Handling Methods [2, 18]: As discussed in the manuscript, the outlier handling methods [2, 18] mainly focus on the non-blind image deblurring, and both approaches use the blind deblurring method [1] to estimate blur kernels on the image patches without outliers. However, it is difficult to select a good image patch when the outliers are uniformly distributed in a blurred image (*e.g.*, impulse noise). Without good kernel estimates, clear latent images cannot be recovered well [2, 18]. In the manuscript, we show that our method improves kernel estimation of [1], which accordingly improves the performance of [2, 18]. We note that [2] involves an outlier detection step as an EM approach is developed. To further clarify the difference, we use our kernel estimates together with the outlier detection result of [2] for fair comparisons. The results are shown in Figure 3. As the proposed outlier detection method is gradually refined in a coarse-to-fine framework (See Figure 2), it is able to detect the outliers and more robust than [2]. In contrast, method [2] is not able to detect some saturated regions as shown in Figure 3(b).

Effectiveness of Proposed Final Latent Image Estimation: The proposed final latent image estimation is in spirit similar to the proposed outlier detection method. We note that the weight of the first term in (16) in the manuscript is the outlier detection function. Therefore, it is able to detect outliers and facilitates the latent image restoration (See Figure 4).

*Corresponding author.

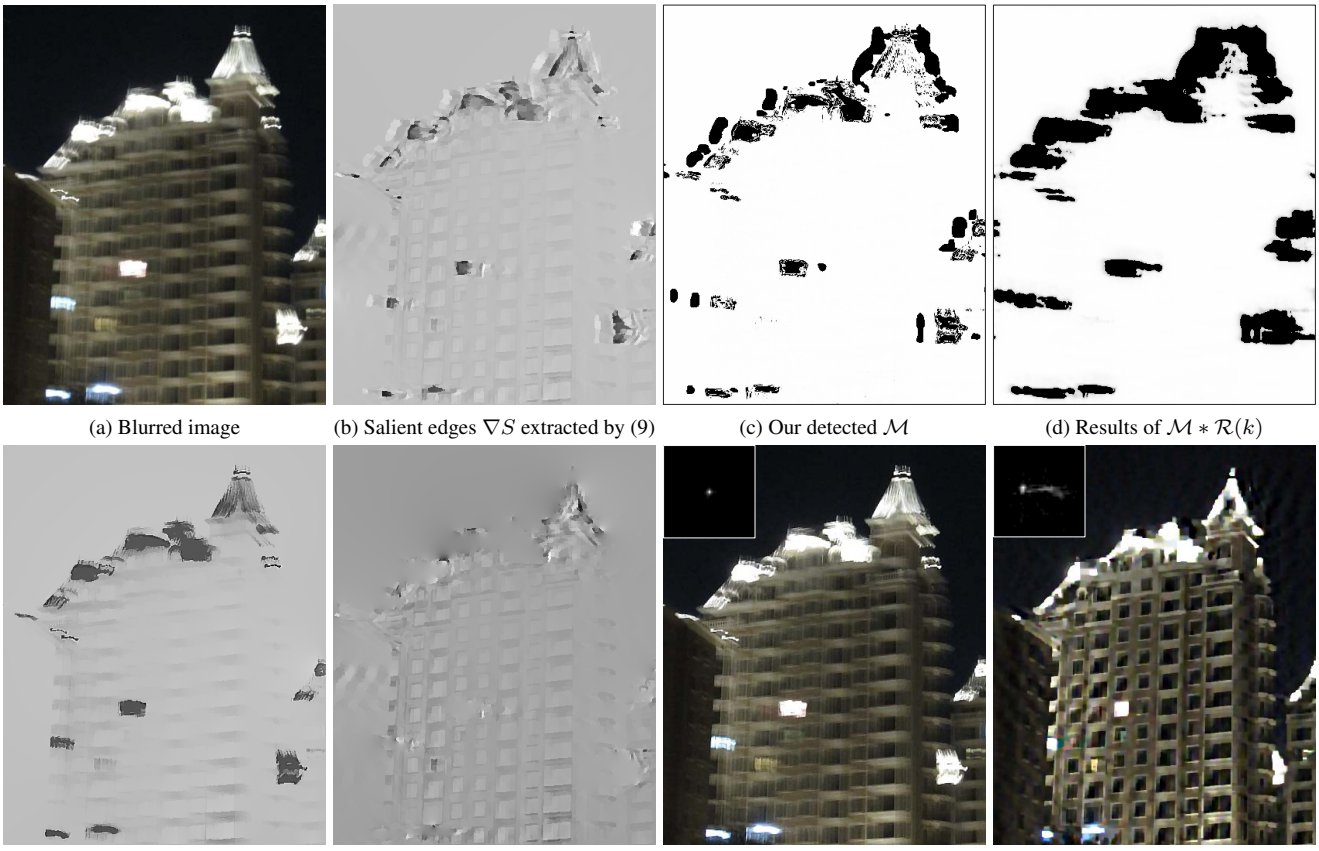

(a) Blurred image (b) Salient edges ∇S extracted by (9) (c) Our detected $\mathcal{M}$ (d) Results of $\mathcal{M} * \mathcal{R}(k)$

(e) Salient edges without using $\mathcal{M}$ (f) Salient edges by applying (d) (g) Our results without using $\mathcal{M}$ (h) Our results using $\mathcal{M}$

Figure 1. Effectiveness of the proposed method. The proposed method first extracts salient edges from intermediate latent images. However, as saturated areas in the blurred image are salient (*e.g.*, the white blobs), these areas are likely to be selected as shown in (b). The proposed outlier detection method is able to detect the outliers and remove them from (b). Thus, only the edges without outliers, *i.e.*, (f), are used for kernel estimation. As mentioned in the manuscript, the positions of dark regions in $\mathcal{M}$ do not always correspond to the positions of outliers in an intermediate edge extracted by (9) due to the influences of blur. The use of $(\mathcal{M} * \mathcal{R}(k))$ (*i.e.*, (d)) makes the positions of dark regions in $\mathcal{M}$ cover the positions of outliers in intermediate edges, and thus remove outliers from (b) (See (f)). The results shown in (g) and (h) demonstrate that the proposed method is able to estimate blur kernels from blurred images with significant outliers. The results shown in (c) and (d) are visualized by binary images of original results for better visual comparisons.

2. Improving Existing Deblurring Methods

In image deblurring literatures, there are three well known approaches based on edge predictions (*e.g.*, [1, 20]), MAP estimations (*e.g.*, [16, 11, 21]), and variational Bayesian inference (*e.g.*, [4, 13, 12]). Since the former two approaches involve the intermediate latent image estimation step, we evaluate the proposed algorithm against the corresponding state-of-the-art methods. As mentioned in the manuscript, the proposed outlier detection method can be used to improve the performance of existing edge prediction based deblurring methods (*e.g.*, [1]). In this supplemental material, we choose one state-of-the-art MAP based method [21] to demonstrate that the proposed method can also be used to improve the performance of existing MAP based deblurring methods to handle images with outliers.

2.1. Synthetic Images

We use the same datasets as mentioned in the manuscript for evaluation. Since the intermediate latent image restoration step of [21] adopts the L_0-regularized gradient prior, the recovered intermediate latent image I only contains large structures. That is, the result of $I * k$ is significantly different from the blurred image B. To apply our algorithm, we use the non-blind deconvolution method [13] to generate an intermediate latent image with the estimated kernel from [21], and then use (12) of the manuscript to compute $\mathcal{M}$. The results shown in Figure 5(b) demonstrate the merits of the proposed method. Figure 6

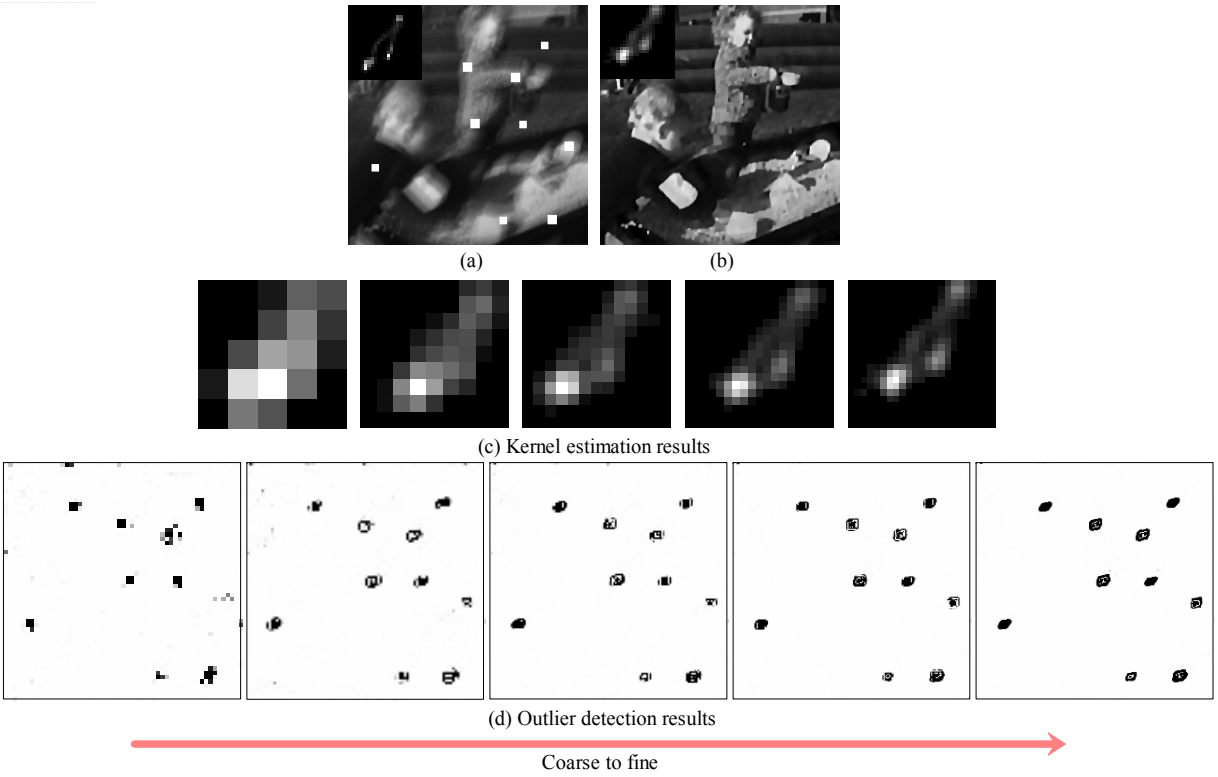

Figure 2. Coarse-to-fine outlier detection results from a synthetic example. (a) Blurred image and kernel. (b) Our results. (c)-(d) Estimated kernels and $\mathcal{M}$ over iterations.

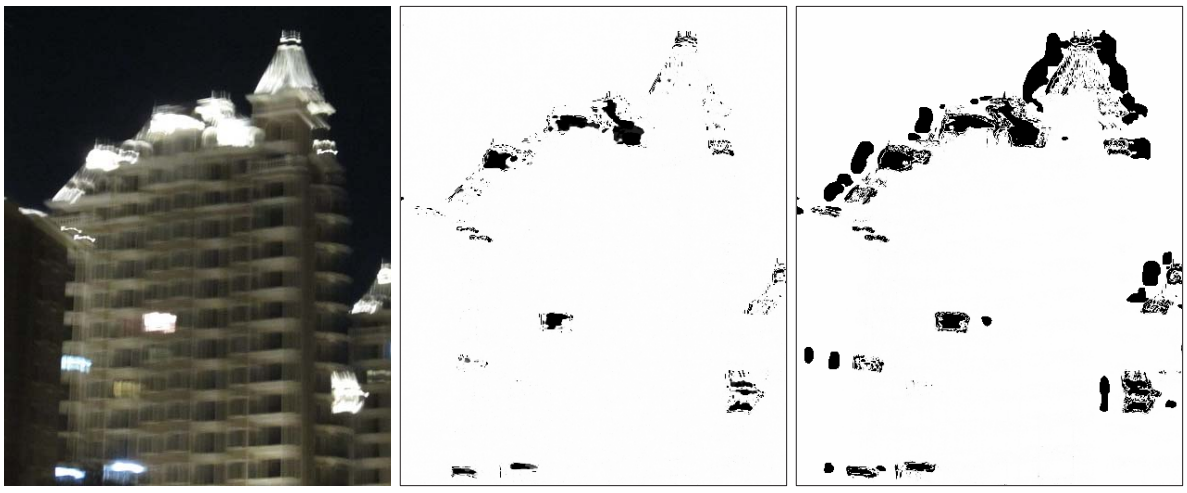

Figure 3. Difference from outlier handling method [2]. As discussed in the manuscript, the outlier handling method [2] mainly focuses on the non-blind image deblurring. We note that [2] involves an outlier detection step as an EM approach is developed. To further clarify the difference of outlier detection method, we use our kernel estimate as the input of [2]. Method [2] is not able to detect some saturated regions as shown in (b). In contrast, as the proposed outlier detection method is gradually refined in a coarse-to-fine framework (See Figure 2), it is able to detect the saturated areas and more robust than [2].

shows the estimated kernels by the state-of-the-art methods with and without $\mathcal{M}$.

(a) Blurred image & estimated kernel (b) TV-ℓ_1 [20] (c) Whyte *et al*. [18] Cho *et al*. [2] Ours

Figure 4. Effectiveness of the proposed final latent image estimation. The proposed final latent image estimation is in spirit similar to the proposed outlier detection method. We note that the weight of the first term in (16) in the manuscript is the outlier detection function. Therefore, it is able to detect outliers and facilitates the latent image restoration. The recovered image by the proposed method contains much clearer characters.

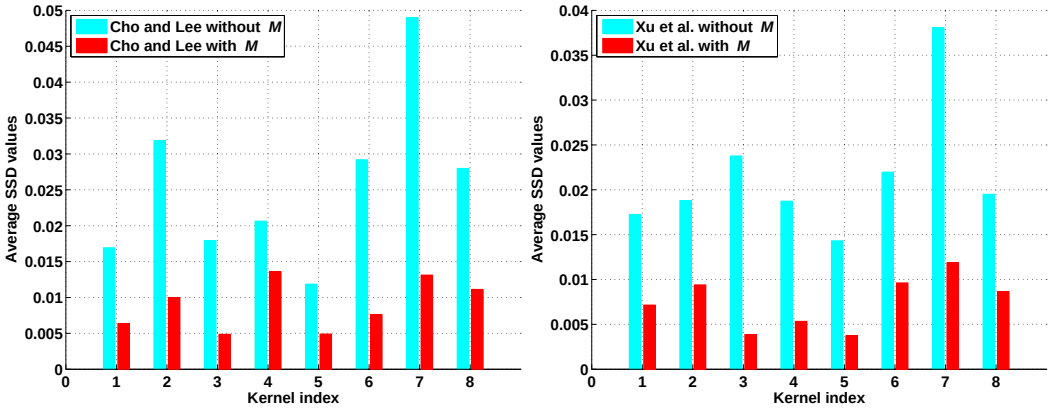

(a) Improvement of Cho and Lee [1] (b) Improvement of Xu *et al*. [21]

Figure 5. Improvement of existing deblurring methods on synthetic datasets. The edge prediction based deblurring method [1] and the state-of-the-art MAP based method [21] fail to generate blur kernels from blurred images due to the influence of outliers. The generated kernel estimates have high SSD values. However, the performance of these two methods is greatly improved using the proposed outlier detection method.

2.2. Real Images

We also use real images to evaluate the proposed method. Figure 7(a) shows a real blurred image which is obtained from [18]. Due to saturated areas, the deblurring methods [1, 21] do not estimate kernels well. However, the performance of these methods is greatly improved with the mask from the proposed algorithm (See Figure 7(d) and (f)).

3. Limitations of the Proposed Method

Our method has the same limitations as state-of-the-art edge-based deblurring methods and is likely to fail when edges are not extracted. Figure 8 shows an example, where the proposed method fails to extract useful edges for kernel estimation.

4. Quantitative Evaluation on Datasets with Outliers

Datasets with Saturated Areas: We create a dataset containing 10 ground truth images with saturated regions and 8 kernels from [12]. The size of the saturated regions in this dataset is from 5×5 to 400×400 pixels. Similar to [8], we stretch the intensity histogram range of each image into $[0, 2]$ and apply 8 different blur kernels to generate blurred images where the pixel intensities are clipped into the range of $[0, 1]$. Finally, we add 1% random noise on each blurred image. For fair comparison, we use the non-blind deblurring method [8] to generate the final deblurred results. Figure 9 shows that the proposed algorithm achieves favorable results compared to state-of-the-arts.

Datasets with Salt and Pepper Noise: We also evaluate the proposed method on the dataset with salt and pepper noise as it is one of the most common outliers. We add the salt and pepper noise on each image in the dataset by Levin *et al*. [12],

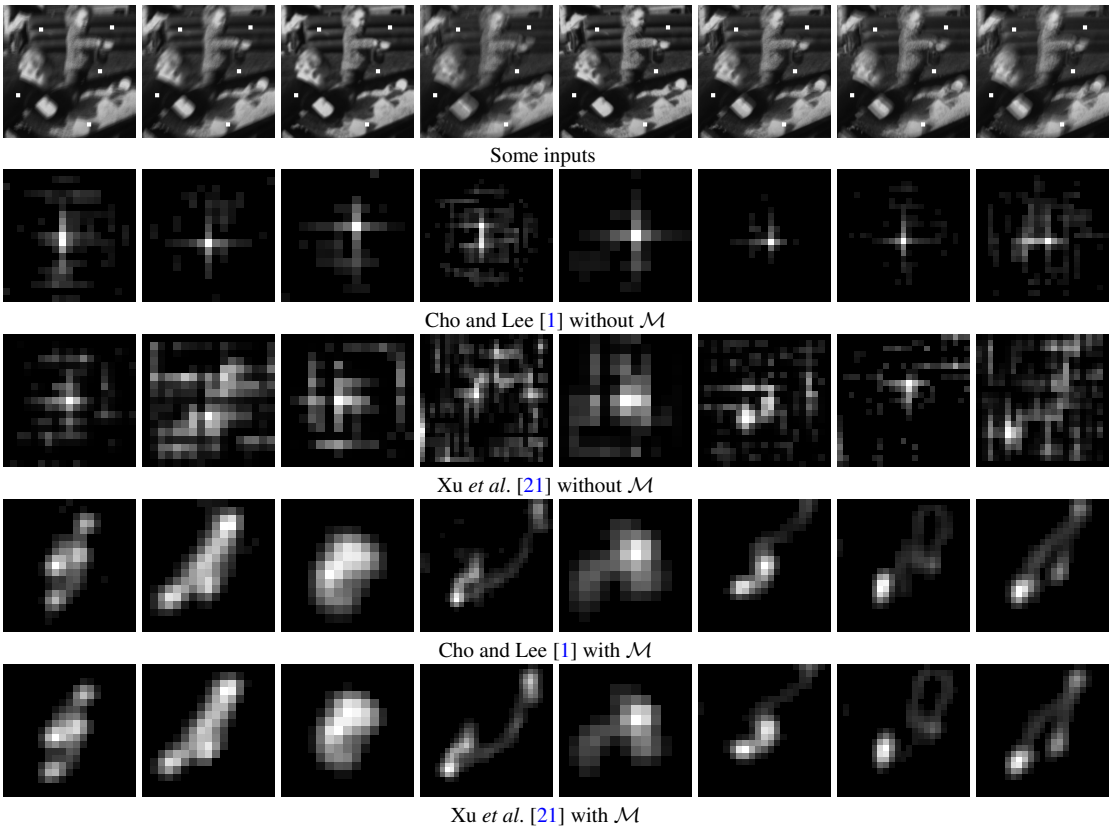

Figure 6. Improvement of existing deblurring methods on synthetic datasets. The edge prediction based deblurring method [1] and the state-of-the-art MAP based method [21] fail to generate blur kernels from blurred images as shown in the second and third rows due to the influence of outliers. However, the performance of these two methods is greatly improved using the proposed outlier detection method.

where the noise density is set to be 0.01. The error ratio metric [12] is used for quantitative evaluations. Figure 10 shows that the proposed algorithm achieves favorable results.

Robustness to Outliers: We further evaluate the proposed method on the images with different noise densities. Figure 11 shows that the proposed algorithm performs well even when the noise density is high.

5. Robustness to Different Kinds of Noise

In the manuscript, we show that the proposed method is robust to salt and pepper noise. To evaluate the performance of the proposed algorithm with respect to random/Gaussian noise presented in [22], we collect 5 images and add the random noise with the levels from 1% to 5%. Using the test dataset with 25 images, we evaluate the proposed algorithm against the state-of-the-art deblurring methods [1, 11] and noisy image deblurring method [22]. For fair comparisons of kernel estimates, we use the non-blind deconvolution method [22] to generate the final deblurred results. The results in Figure 12 show that the proposed algorithm performs favorably against the state-of-the-art noisy image deblurring method [22] with higher PSNR values.

6. Quantitative Evaluation on the Natural Image Deblurring Datasets [10], [12], and [17]

We evaluate our method on the natural image deblurring datasets [12] and [10]. The natural image deblurring datasets [12] contains 4 ground truth images and 8 blur kernels. Figure 13(a) shows the cumulative histogram of the deconvolution error ratio across test examples. The proposed method achieves 96.78% of the results under error ratio 2.

Similar to [10], we employ PSNR to evaluate the results on the dataset [10]. Figure 13(b) demonstrates that the proposed algorithm performs favorably against the state-of-the-art methods. Figure 14 shows one example from the dataset [10].

(a) Blurred image

(b) Hu *et al*. [8]

(c) Cho and Lee [1]

(d) Cho and Lee [1] with $\mathcal{M}$

(e) Xu *et al*. [21]

(f) Xu *et al*. [21] with $\mathcal{M}$

Figure 7. Improvement of existing deblurring methods on real challenging images. The edge prediction based deblurring method [1] and the state-of-the-art MAP based method [21] fail to generate blur kernels from blurred images as shown in (c) and (e) due to the influence of outliers. However, the performance of these two methods is greatly improved using the proposed outlier detection method.

(a) Blurred image (b) Intermediate extracted salient edges (c) Ours

Figure 8. The proposed method is likely to fail when edges are not extracted from intermediate latent images.

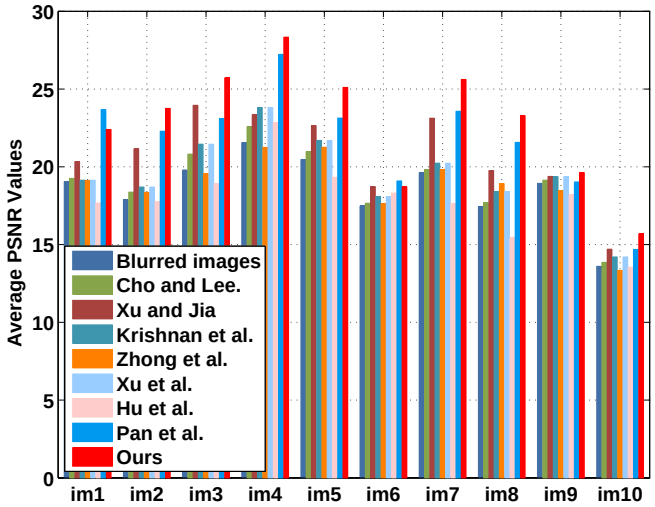

Figure 9. Quantitative evaluation on the dataset with saturated regions. The dataset contains 10 ground truth images with saturated regions and 8 kernels from [12]. The size of the saturated regions in this dataset is from 5×5 to 400×400 pixels. we use the non-blind deblurring method [8] to generate the final deblurred results for fair comparisons. The proposed algorithm achieves favorable results compared to the state-of-the-art methods.

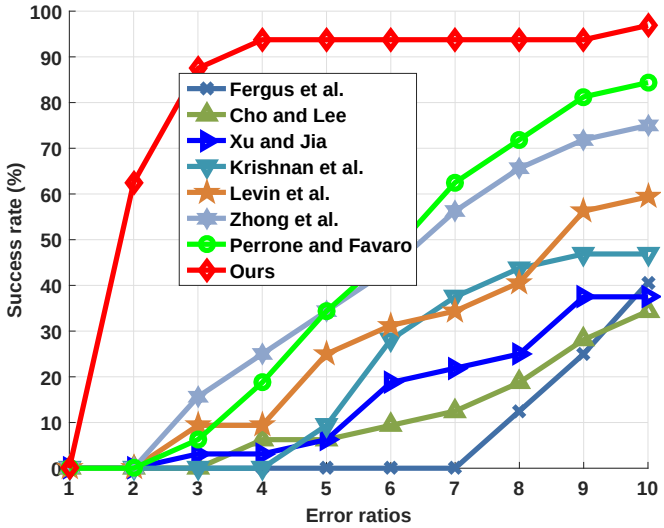

Figure 10. Quantitative evaluation on the dataset with salt and pepper noise. We add the salt and pepper noise (which is one of the most common outliers) on each image in the dataset by Levin *et al.* [12], where the noise density is set to be 0.01. The kernel similarity metric [9] is used for quantitative evaluations. The proposed algorithm achieves favorable results with higher kernel similarity values.

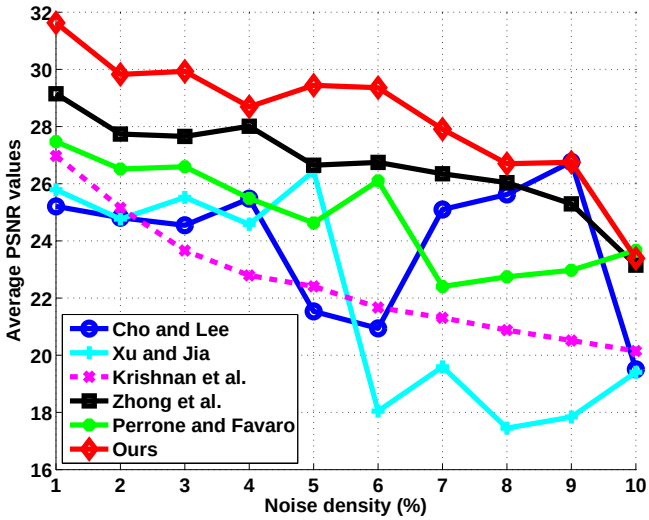

Figure 11. Robustness to outliers. As the proposed method is able to deal with outliers, we evaluate it on the images with noise density of salt and pepper noise from 1% to 10%. The results show that the proposed algorithm performs well even when the noise density is high.

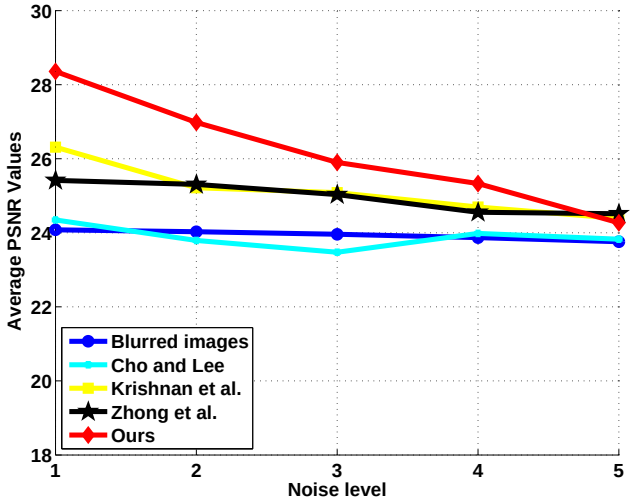

Figure 12. Robustness to the random noise. Although the proposed method is designed for outliers, it is able to deal with random noise to a certain extent. To evaluate the performance of the proposed algorithm with respect to random/Gaussian noise presented in [22], we collect 5 images and add the random noise with the levels from 1% to 5%. Using the test dataset with 25 images, we evaluate the proposed algorithm against the state-of-the-art deblurring methods [1, 11] and noisy image deblurring method [22]. For fair comparisons of kernel estimates, we use the non-blind deconvolution method [22] to generate the final deblurred results. The results show that the proposed algorithm performs well even when the noise level is high.

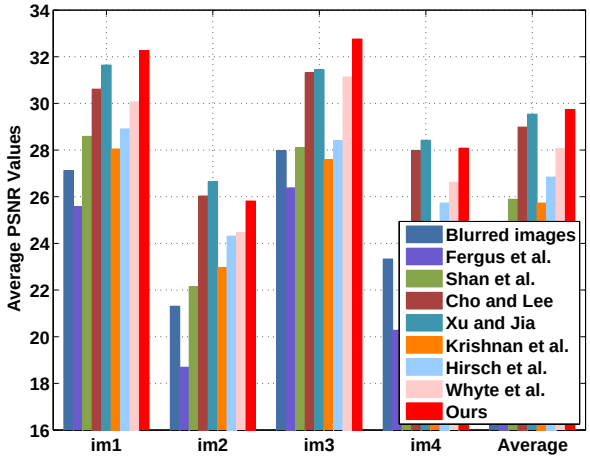

(a) Results on dataset by Köhler *et al*. [10]

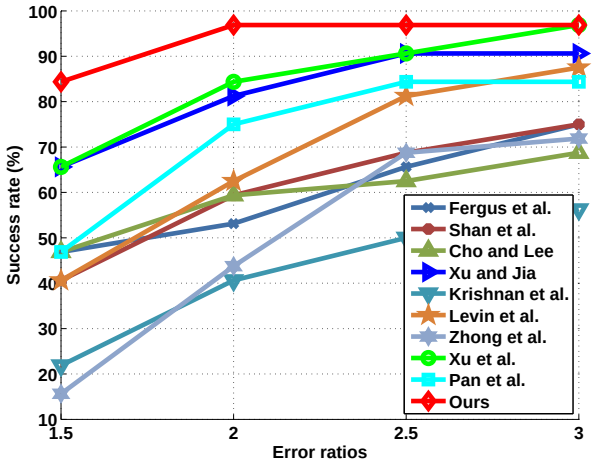

(b) Results on dataset by Levin *et al*. [12]

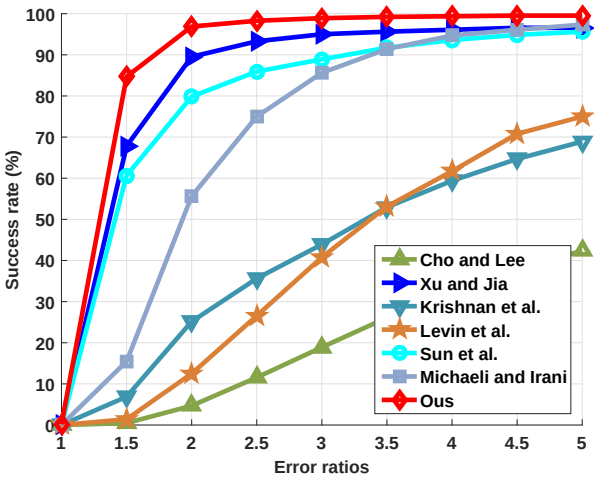

(c) Results on dataset by Sun *et al*. [17]

Figure 13. Quantitative evaluations on natural image deblurring datasets without outliers. As mentioned in the manuscript, the algorithm can be applied to deblur natural images without outliers. We quantitatively evaluate the proposed method on benchmark datasets [12, 10, 17]. The results show that the proposed algorithm performs well on both datasets against the state-of-the-art deblurring methods.

(a) Blurred image (b) Fergus *et al*. [4] (c) Shan *et al*. [16]

(d) Cho and Lee [1] (e) Xu and Jia [21] (f) Krishnan *et al*. [11]

(g) Hirsch *et al*. [7] (h) Whyte *et al*. [19] (i) Ours

Figure 14. Deblurred results using one example from natural image dataset [10]. Our method generates much clearer results. All the deblurred results are included in the attached "*code*" folder.

7. More Experimental Results

In this section, we show more deblurred results by the proposed algorithm and the state-of-the-art methods.

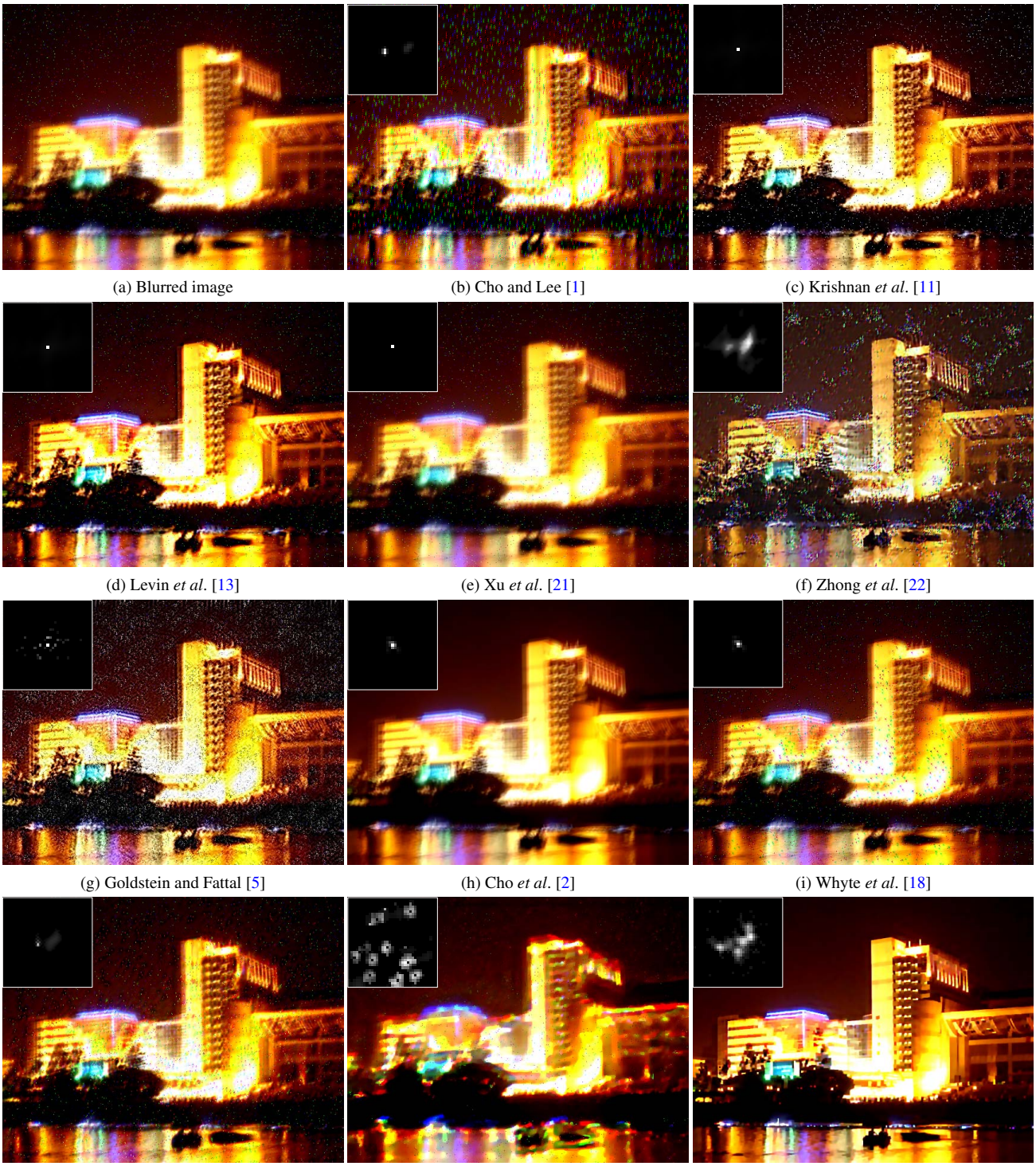

(a) Blurred image (b) Cho and Lee [1] (c) Krishnan *et al*. [11]

(d) Levin *et al*. [13] (e) Xu *et al*. [21] (f) Zhong *et al*. [22]

(g) Goldstein and Fattal [5] (h) Cho *et al*. [2] (i) Whyte *et al*. [18]

(j) Pan *et al*. [15] (k) Hu *et al*. [8] (l) Ours

Figure 15. Deblurred results on one blurred image with numerous saturated areas and noise. Although methods [2, 19] is able to handle outliers, they mainly focus on the non-blind image deblurring. The results show that these methods fail to generate clear images due to the imperfect blur kernels.

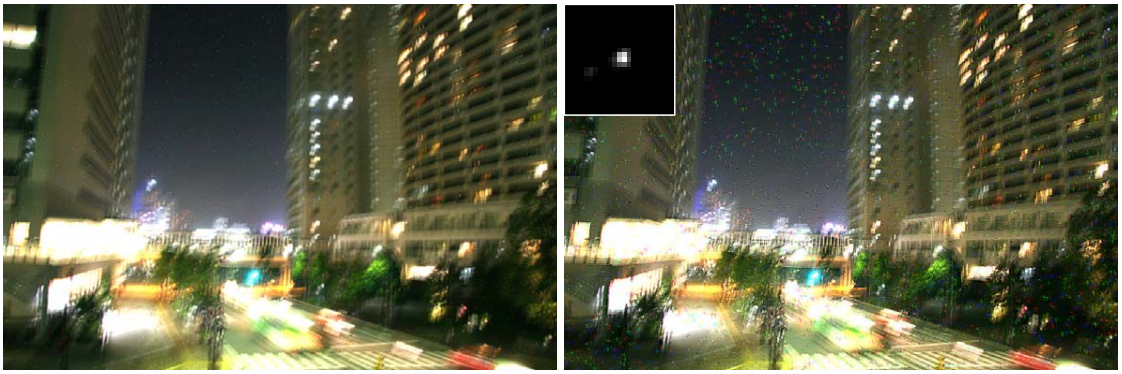

(a) Blurred image

(b) Cho and Lee [1]

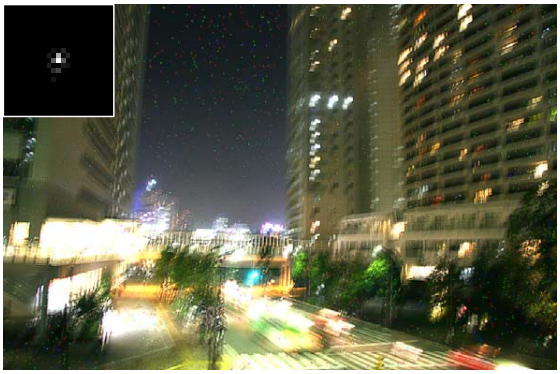

(c) Xu *et al*. [21]

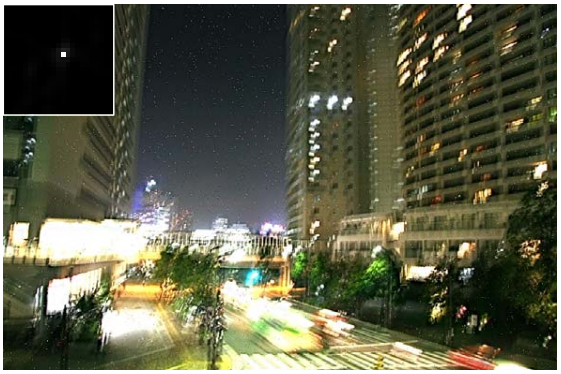

(d) Krishnan *et al*. [11]

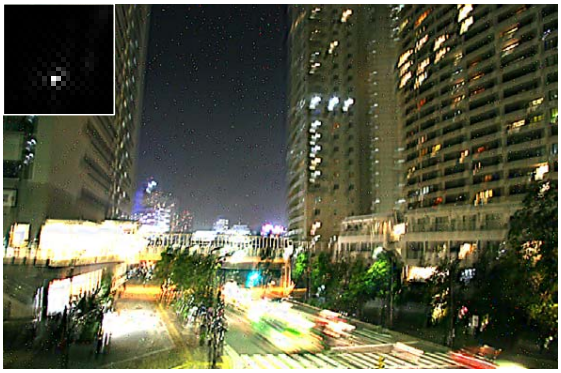

(e) Levin *et al*. [13]

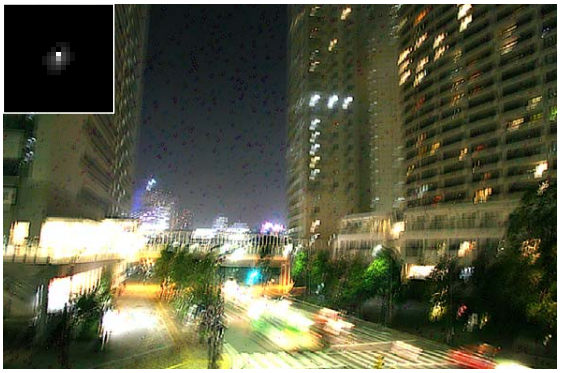

(f) Pan *et al*. [15]

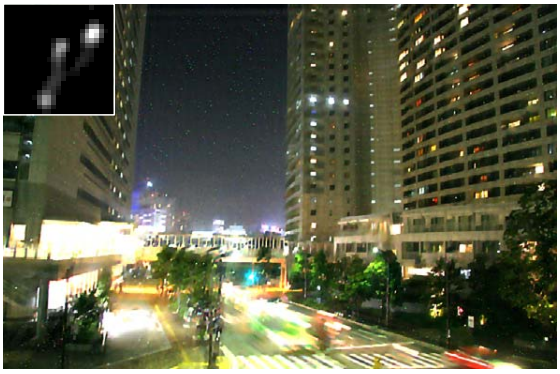

(g) Hu *et al*. [13]

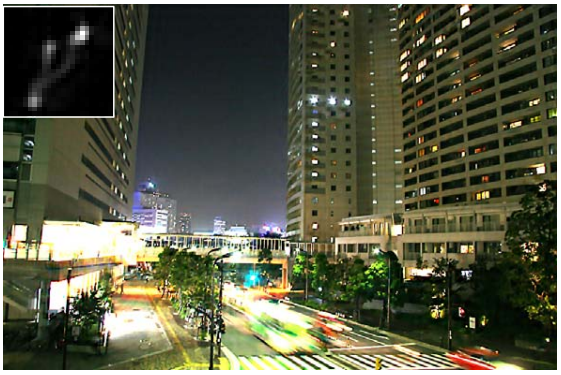

(h) Ours

Figure 16. Deblurred results on one blurred image with saturated regions and impulse noise from [2]. Our method generates a clear image with fine details.

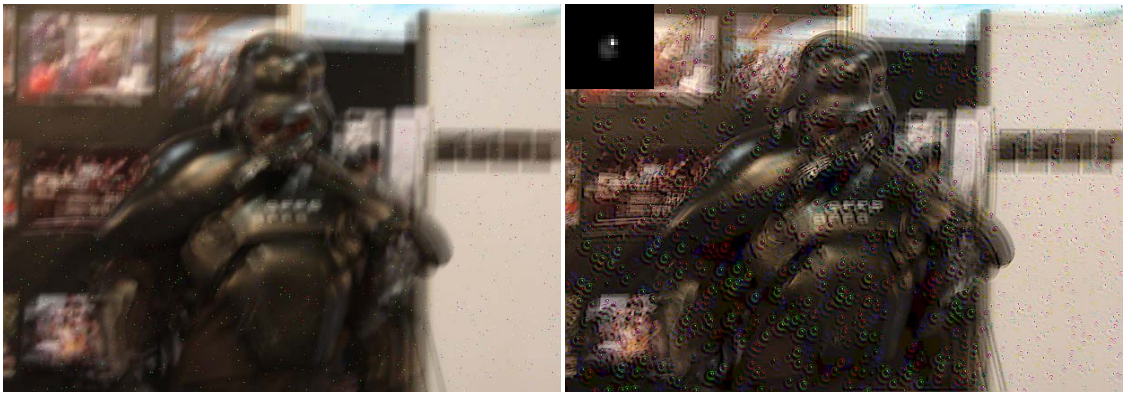

(a) Blurred image (b) Cho and Lee [1]

(c) Xu *et al*. [21] (d) Krishnan *et al*. [11]

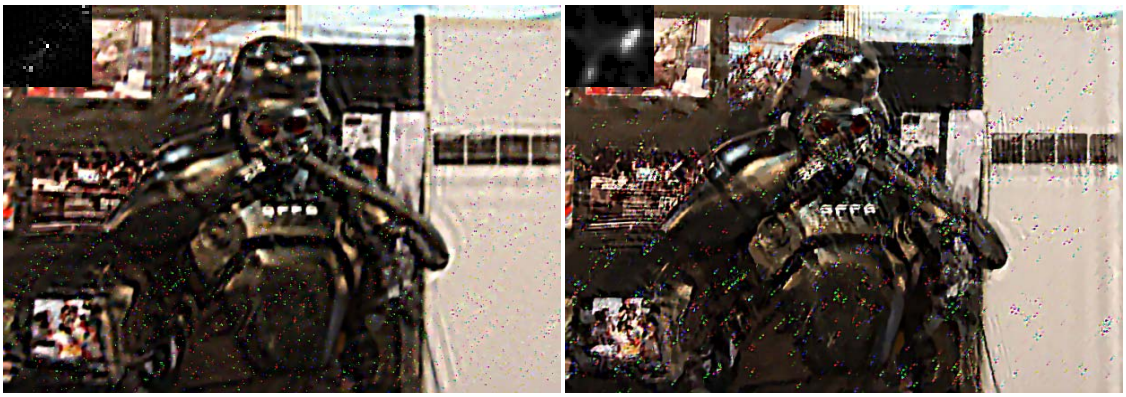

(e) Levin *et al*. [13] (f) Zhong *et al*. [22]

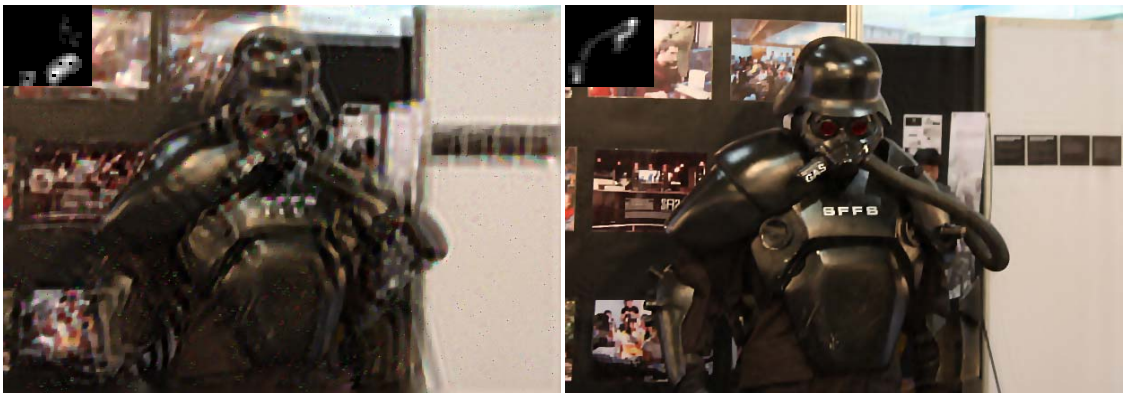

(g) Hu *et al*. [8] (h) Ours

Figure 17. Deblurred results on one blurred image with large noise from [2]. Our method generates a much clearer image.

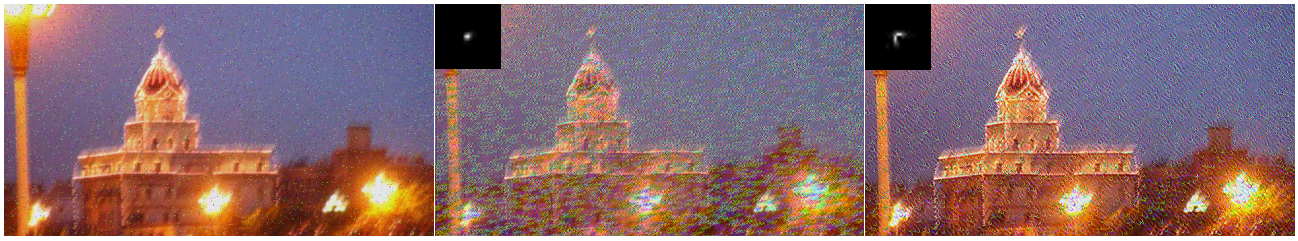

(a) Blurred image (b) Shan *et al*. [16] (c) Cho and Lee [1]

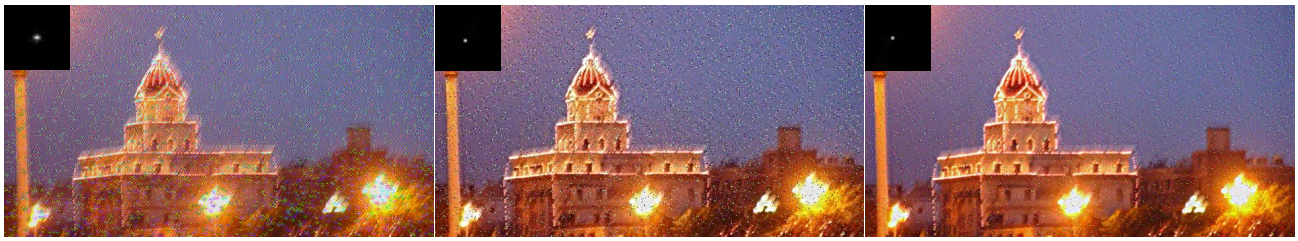

(d) Xu and Jia [20] (e) Krishnan *et al*. [11] (f) Levin *et al*. [13]

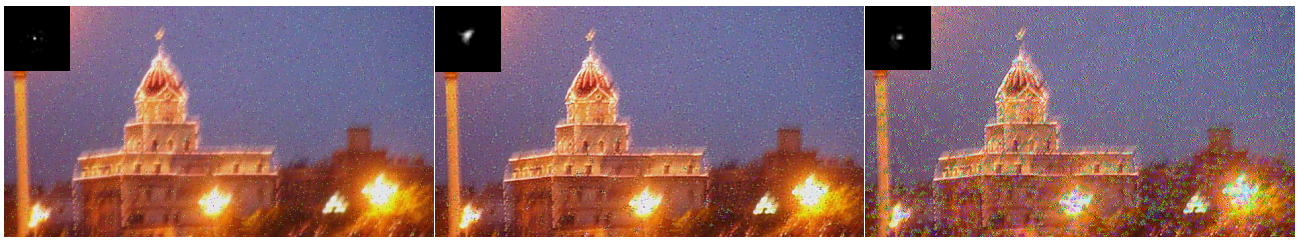

(g) Goldstein and Fattal [5] (h) Zhong *et al*. [22] (i) Xu *et al*. [21]

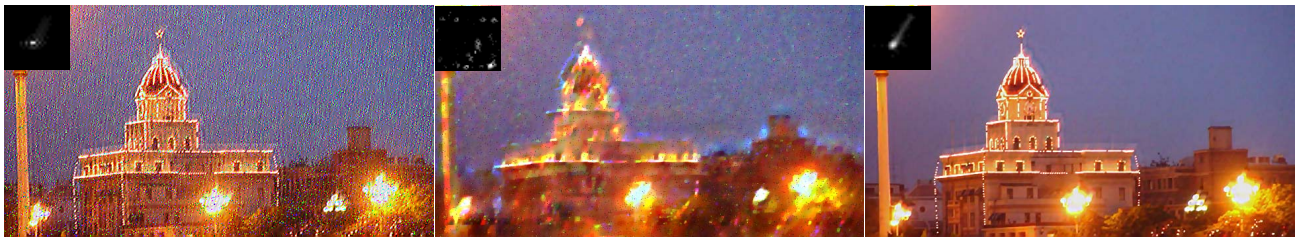

(j) Pan *et al*. [15] (k) Hu *et al*. [8] (l) Ours

Figure 18. Deblurred results on one blurred image with large saturated areas (*e.g*., light blobs) and noise. State-of-the-art deblurring algorithms [16, 1, 20, 11, 13, 5, 22, 21, 15, 8] fail to generate clear images. In contrast, our method generates a clear image with fine details.

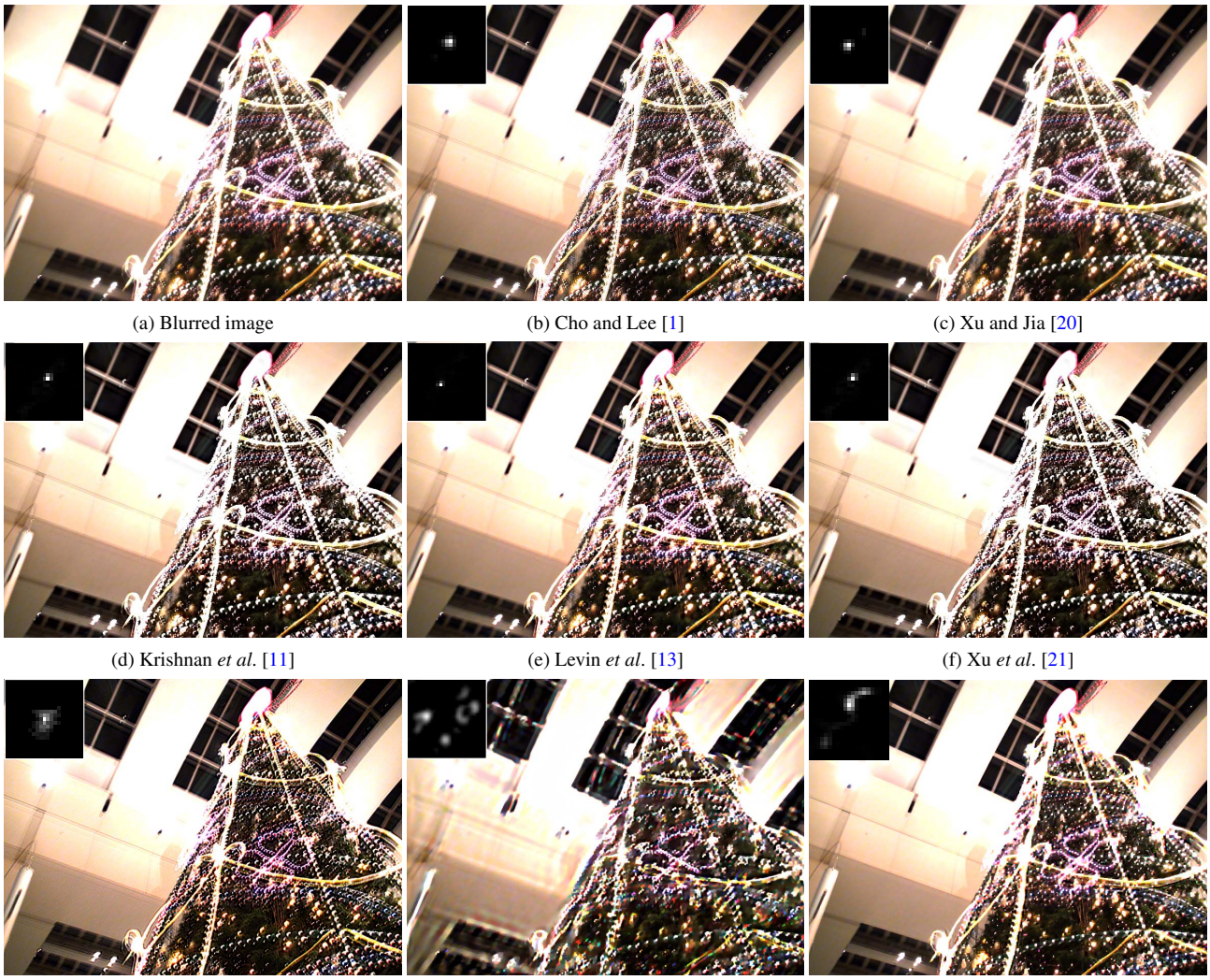

(a) Blurred image (b) Cho and Lee [1] (c) Xu and Jia [20]

(d) Krishnan *et al*. [11] (e) Levin *et al*. [13] (f) Xu *et al*. [21]

(g) Pan *et al*. [15] (h) Hu *et al*. [8] (i) Ours

Figure 19. Deblurred results on one blurred image with saturated areas from [2]. State-of-the-art deblurring algorithms [1, 20, 11, 13, 21, 15, 8] fail to generate clear images. In contrast, our method generates a clear image with fine details.

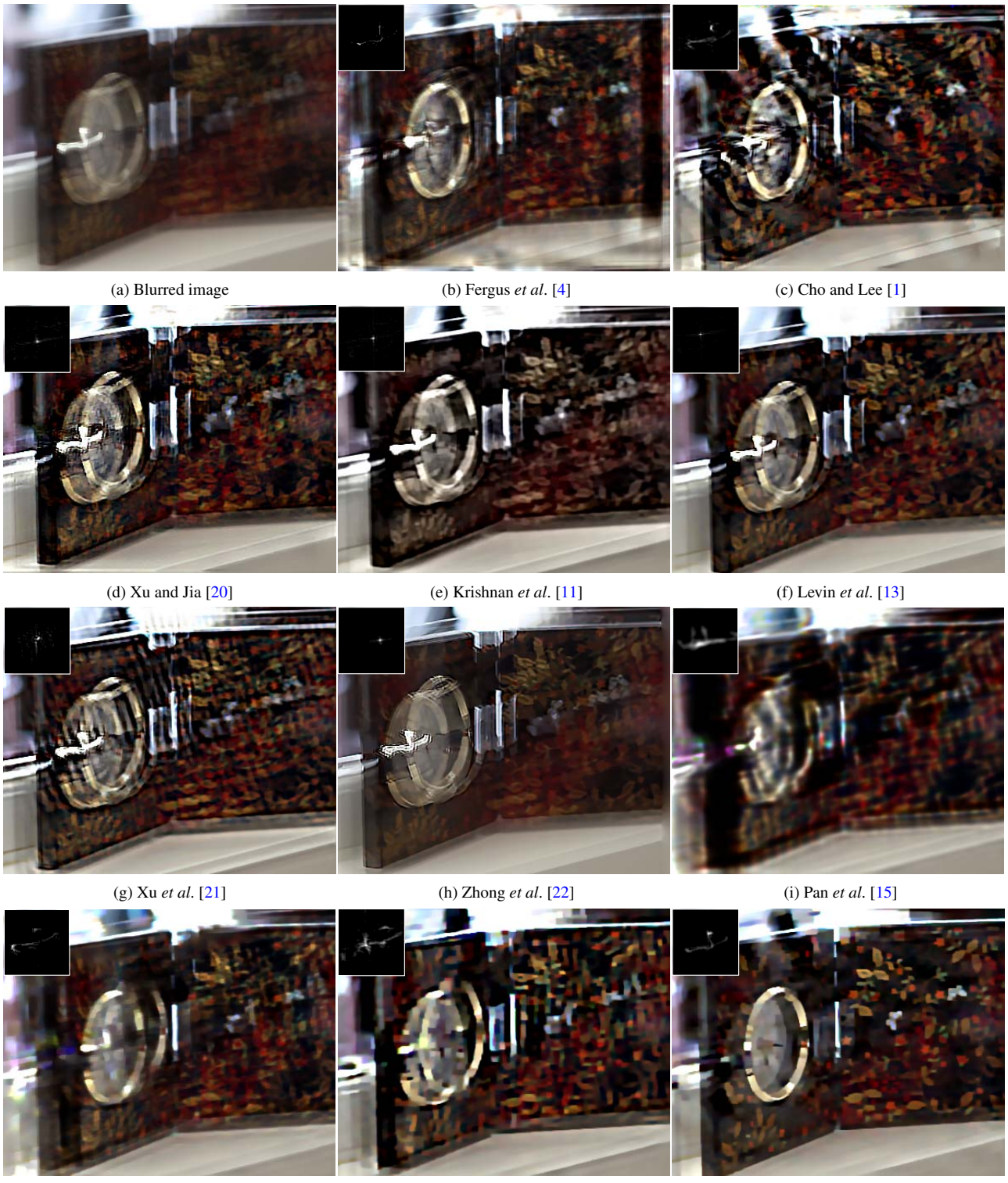

(a) Blurred image (b) Fergus *et al*. [4] (c) Cho and Lee [1]

(d) Xu and Jia [20] (e) Krishnan *et al*. [11] (f) Levin *et al*. [13]

(g) Xu *et al*. [21] (h) Zhong *et al*. [22] (i) Pan *et al*. [15]

(j) Hu *et al*. [8] (k) Ours without $\mathcal{M}$ (l) Ours

Figure 20. Deblurred results on one real captured blurred image with numerous saturated pixels and large blur. State-of-the-art deblurring algorithms [4, 1, 20, 11, 13, 21, 22, 15, 8] fail to generate clear images. In contrast, our method generates a clear image with fine details. Moreover, the comparison results shown in (k) and (l) demonstrate that the proposed algorithm with $\mathcal{M}$ is able to remove outliers in the kernel estimation. The kernel size is estimated at 77×77 pixels.

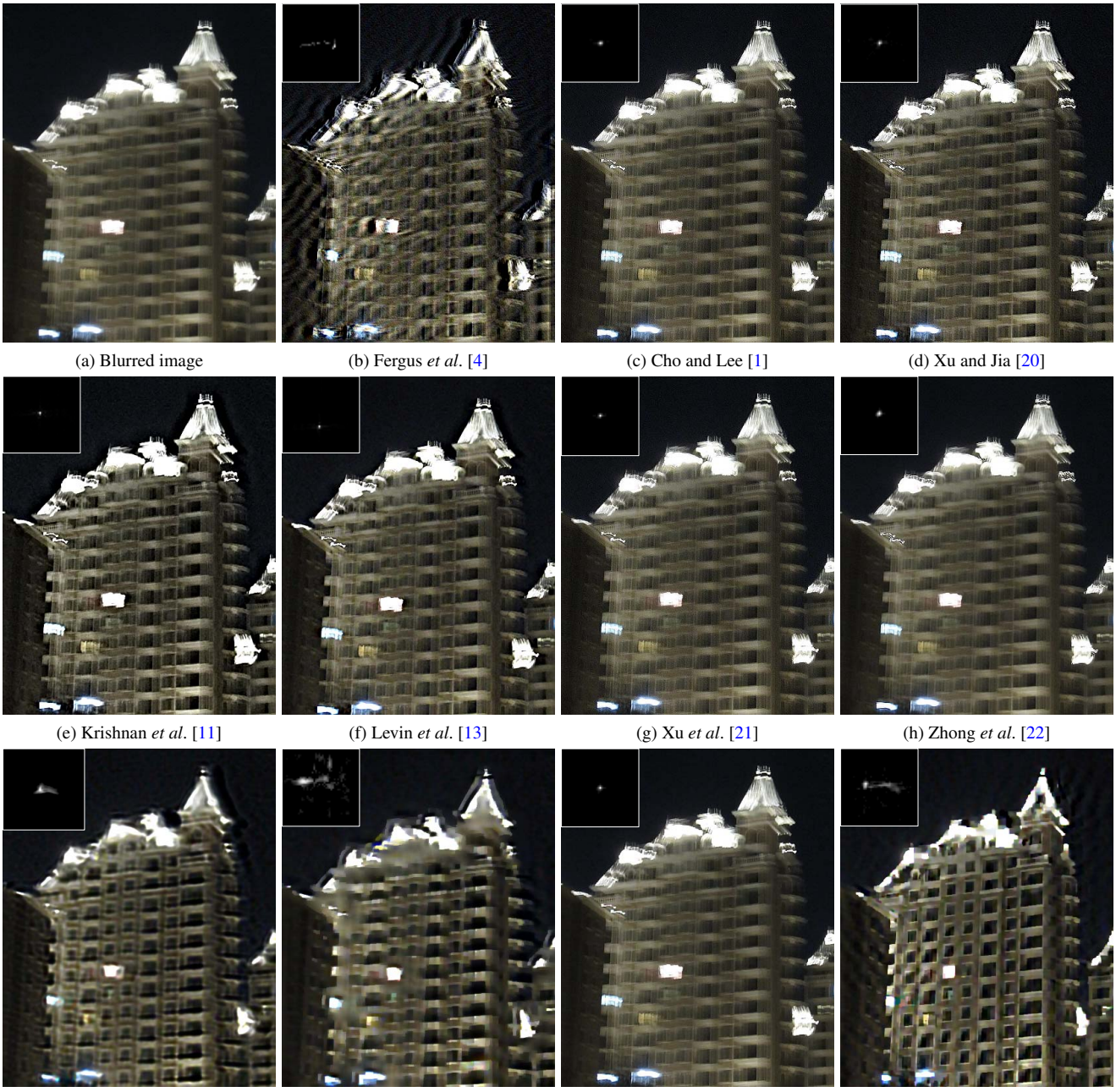

(a) Blurred image (b) Fergus *et al*. [4] (c) Cho and Lee [1] (d) Xu and Jia [20]

(e) Krishnan *et al*. [11] (f) Levin *et al*. [13] (g) Xu *et al*. [21] (h) Zhong *et al*. [22]

(i) Pan *et al*. [15] (j) Hu *et al*. [8] (k) Ours without $\mathcal{M}$ (l) Ours

Figure 21. Deblurred results on one real example with numerous saturated regions (*e.g*., the light blobs). State-of-the-art deblurring algorithms [4, 1, 20, 11, 13, 21, 22, 15, 8] fail to generate clear images. In contrast, our method generates a clear image with fine details. Moreover, the comparison results shown in (k) and (l) demonstrate that the proposed algorithm with $\mathcal{M}$ is able to remove outliers in the kernel estimation. The kernel size is estimated at 45×45 pixels.

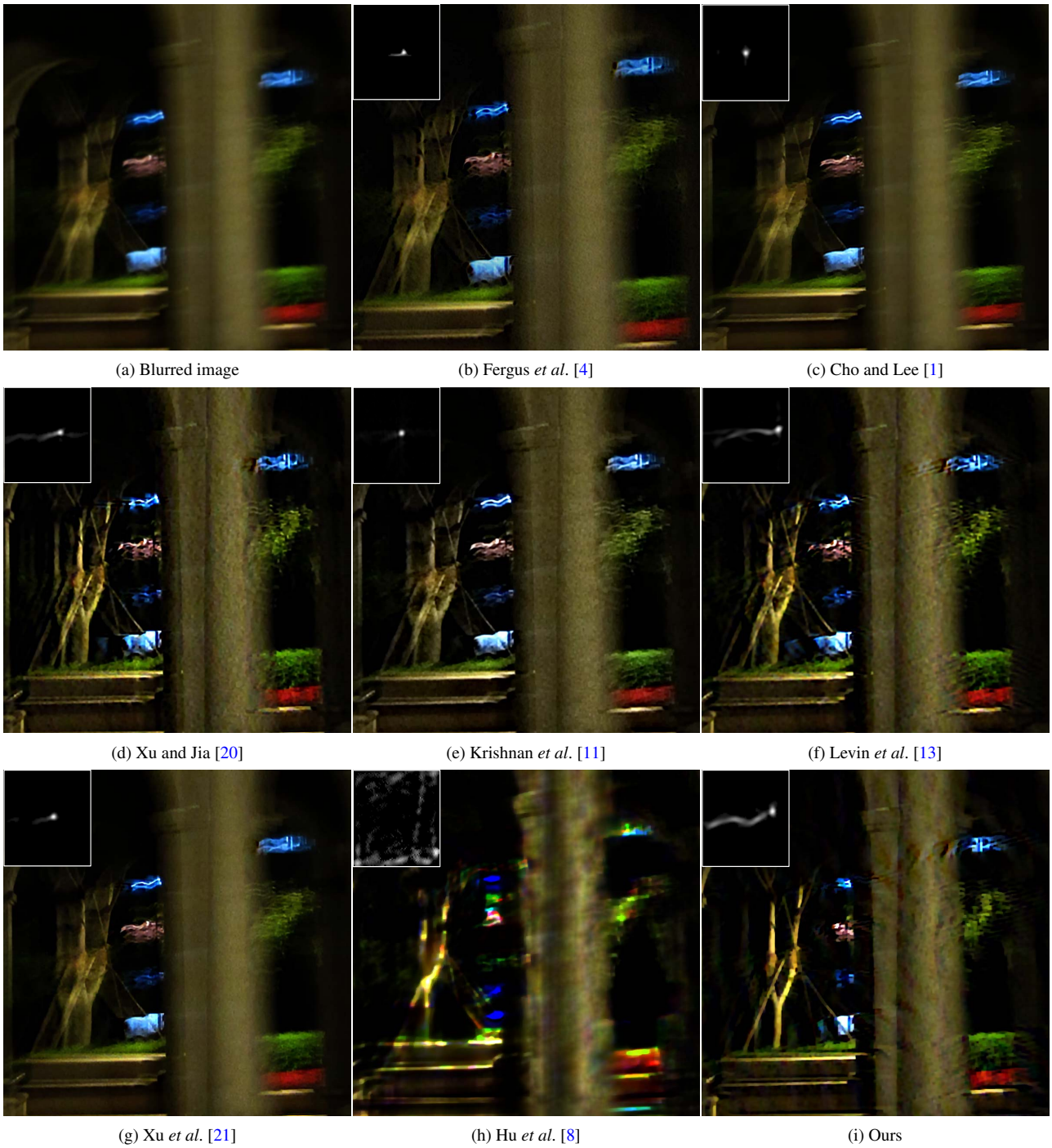

(a) Blurred image (b) Fergus *et al*. [4] (c) Cho and Lee [1]

(d) Xu and Jia [20] (e) Krishnan *et al*. [11] (f) Levin *et al*. [13]

(g) Xu *et al*. [21] (h) Hu *et al*. [8] (i) Ours

Figure 22. Deblurred results on one real example with several light streaks. State-of-the-art deblurring algorithms [4, 1, 20, 11, 13, 21, 8] fail to generate clear images. In contrast, our method generates a clear image with fine details. The kernel size is estimated at 79×79 pixels.

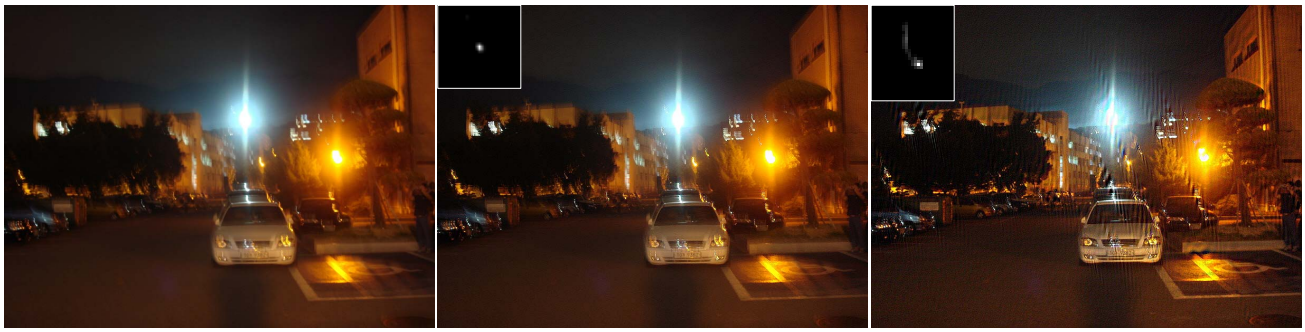

(a) Blurred image (b) Shan *et al*. [16] (c) Cho and Lee [1]

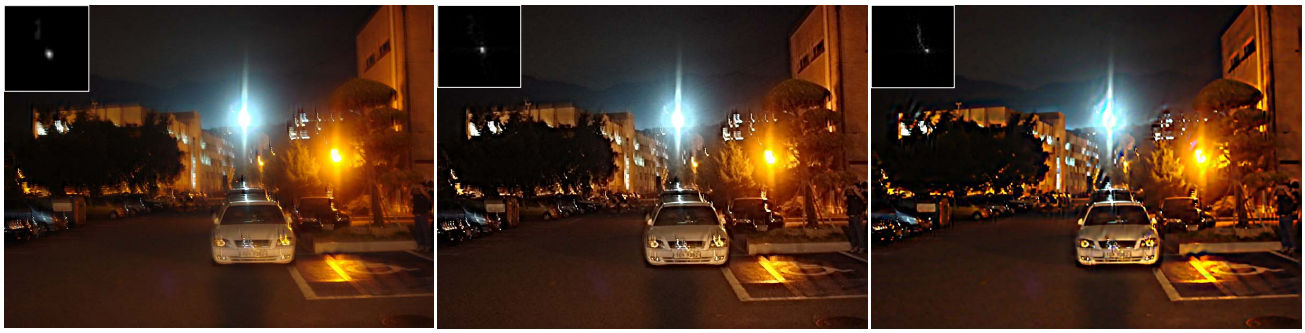

(d) Xu and Jia [20] (e) Krishnan *et al*. [11] (f) Levin *et al*. [13]

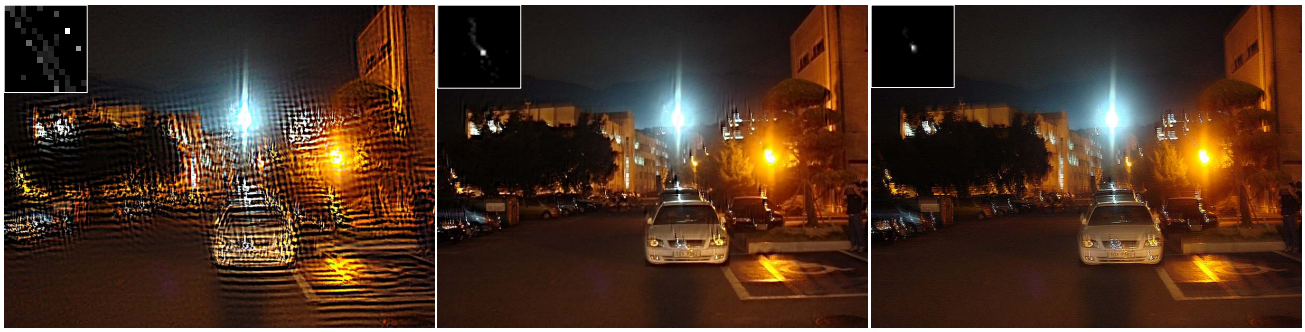

(g) Cho *et al*. [3] (h) Goldstein and Fattal [5] (f) Xu *et al*. [21]

(g) Pan *et al*. [15] (h) Hu *et al*. [8] (i) Ours

Figure 23. Deblurred results on one real example from [1]. Our method generates a much clearer image. The kernel size is estimated at 45×45 pixels.

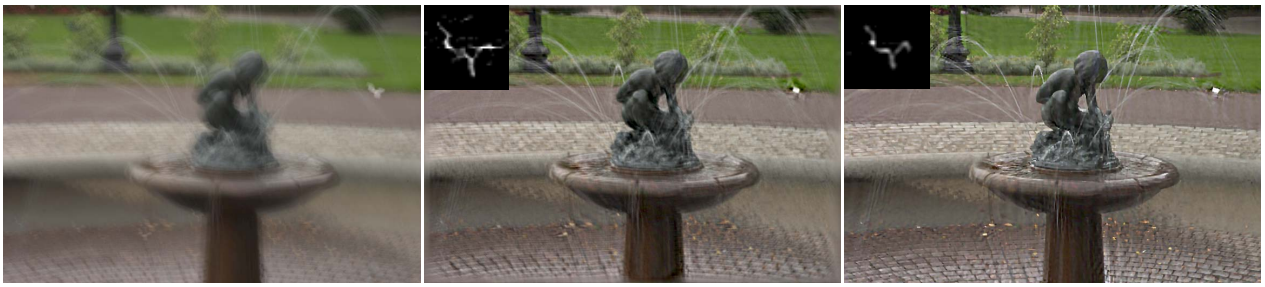

(a) Blurred image (b) Fergus *et al*. [4] (c) Ours

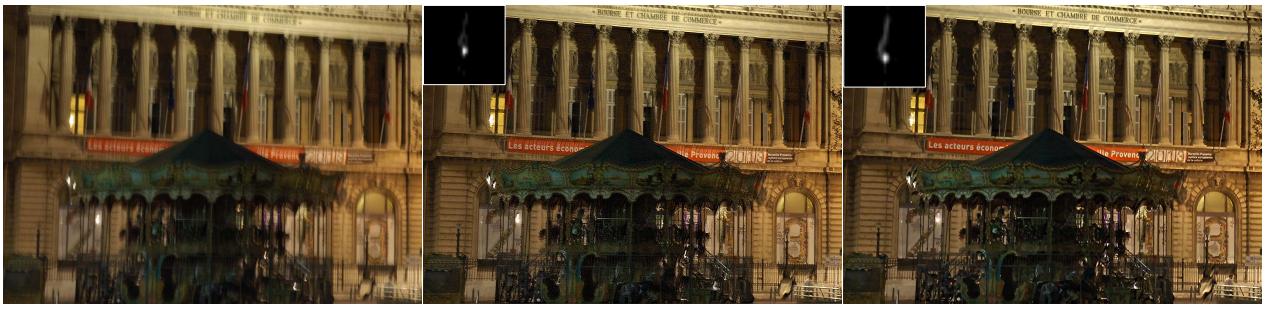

(a) Blurred image (b) Xu and Jia [20] (c) Ours

(a) Blurred image (b) Xu and Jia [20] (c) Ours

(a) Blurred image (b) Xu *et al*. [21] (c) Ours

Figure 24. Comparisons with state-of-the-art deblurring methods. In addition to detect outliers, the proposed algorithm performs well against the state-of-the-art methods on images without significant noise.

(a) Blurred image (b) Xu and Jia [20] (c) Ours

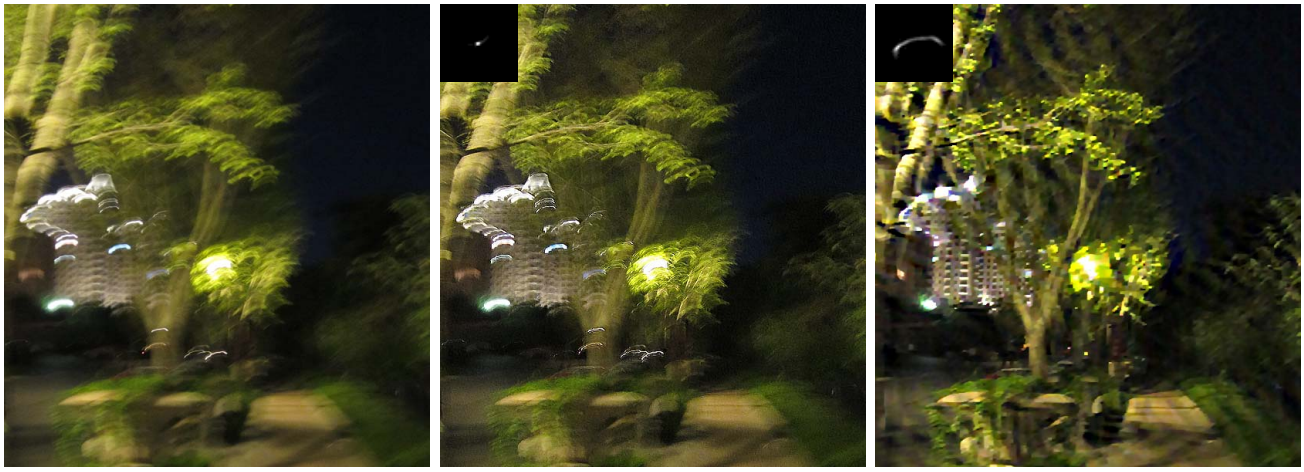

(a) Blurred image (b) Xu *et al*. [21] (c) Ours

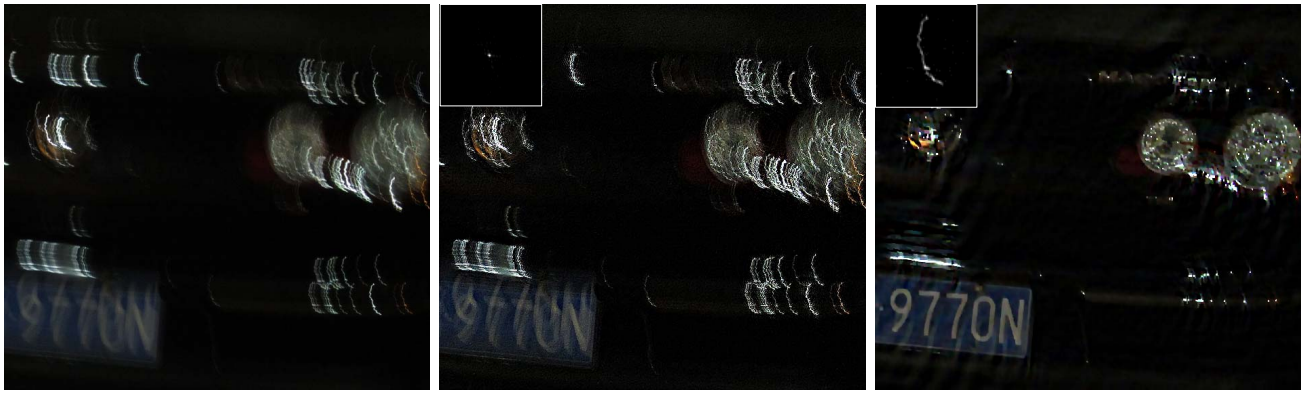

(a) Blurred image (b) Xu and Jia [20] (c) Ours

Figure 25. Comparisons with state-of-the-art deblurring methods. In addition to detect outliers, the proposed algorithm performs well against the state-of-the-art methods on images without significant noise.

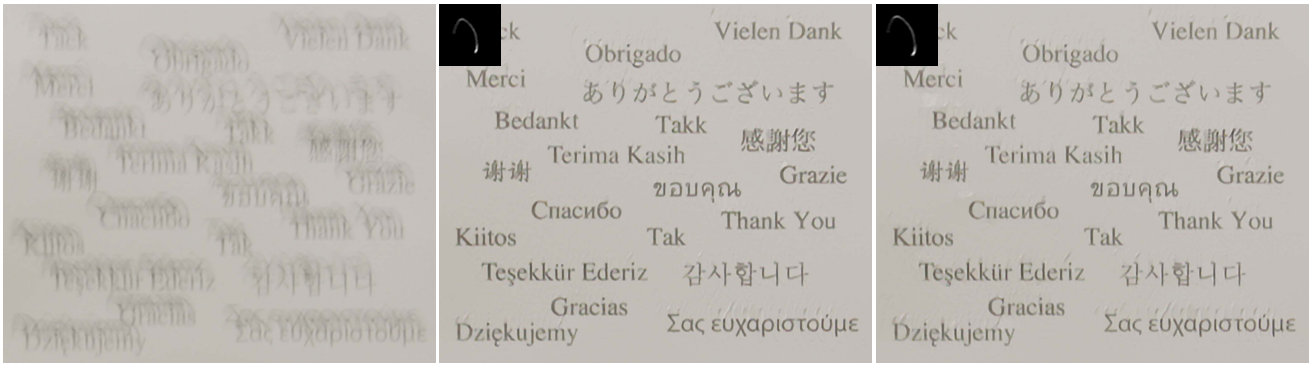

(a) Blurred image (b) Pan *et al*. [15] (c) Our kernel + non-blind deconvolution [15]

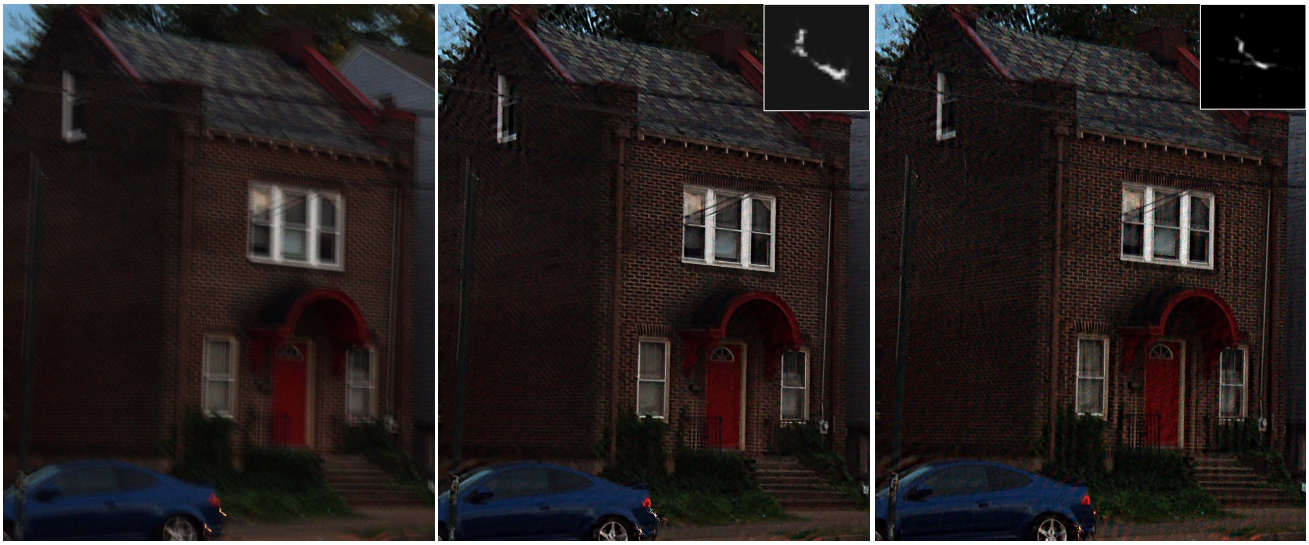

(a) Blurred image (b) Zhong *et al*. [22] (c) Ours

(a) Blurred image (b) Hu *et al*. [8] (c) Ours

Figure 26. Comparisons with state-of-the-art deblurring methods. In addition to detect outliers, the proposed algorithm performs well against the state-of-the-art methods on images without significant noise.

(a) Blurred image (b) Pan *et al*. [14] (c) Ours

(a) Blurred image (b) Gupta *et al*. [6] (c) Ours

(a) Blurred image (b) Whyte *et al*. [19] (c) Ours

Figure 27. Comparisons with state-of-the-art deblurring methods. In addition to detect outliers, the proposed algorithm performs well against the state-of-the-art methods on images without significant noise.

References

[1] S. Cho and S. Lee. Fast motion deblurring. In *SIGGRAPH Asia*, pages 145:1–145:8, 2009. 1, 2, 4, 5, 6, 8, 10, 11, 12, 13, 14, 15, 16, 17, 18, 19

[2] S. Cho, J. Wang, and S. Lee. Handling outliers in non-blind image deconvolution. In *ICCV*, pages 495–502, 2011. 1, 3, 4, 11, 12, 13, 15

[3] T. S. Cho, S. Paris, B. K. P. Horn, and W. T. Freeman. Blur kernel estimation using the radon transform. In *CVPR*, pages 241–248, 2011. 19

[4] R. Fergus, B. Singh, A. Hertzmann, S. T. Roweis, and W. T. Freeman. Removing camera shake from a single photograph. In *SIGGRAPH*, pages 787–794, 2006. 2, 10, 16, 17, 18, 20

[5] A. Goldstein and R. Fattal. Blur-kernel estimation from spectral irregularities. In *ECCV*, pages 622–635, 2012. 11, 14, 19

[6] A. Gupta, N. Joshi, C. L. Zitnick, M. F. Cohen, and B. Curless. Single image deblurring using motion density functions. In *ECCV*, pages 171–184, 2010. 23

[7] M. Hirsch, C. J. Schuler, S. Harmeling, and B. Schölkopf. Fast removal of non-uniform camera shake. In *ICCV*, pages 463–470, 2011. 10

[8] Z. Hu, S. Cho, J. Wang, and M.-H. Yang. Deblurring low-light images with light streaks. In *CVPR*, pages 3382–3389, 2014. 4, 6, 7, 11, 13, 14, 15, 16, 17, 18, 19, 22

[9] Z. Hu and M.-H. Yang. Good regions to deblur. In *ECCV*, pages 59–72, 2012. 7

[10] R. Köhler, M. Hirsch, B. J. Mohler, B. Schölkopf, and S. Harmeling. Recording and playback of camera shake: Benchmarking blind deconvolution with a real-world database. In *ECCV*, pages 27–40, 2012. 1, 5, 9, 10

[11] D. Krishnan, T. Tay, and R. Fergus. Blind deconvolution using a normalized sparsity measure. In *CVPR*, pages 2657–2664, 2011. 2, 5, 8, 10, 11, 12, 13, 14, 15, 16, 17, 18, 19

[12] A. Levin, Y. Weiss, F. Durand, and W. T. Freeman. Understanding and evaluating blind deconvolution algorithms. In *CVPR*, pages 1964–1971, 2009. 1, 2, 4, 5, 7, 9

[13] A. Levin, Y. Weiss, F. Durand, and W. T. Freeman. Efficient marginal likelihood optimization in blind deconvolution. In *CVPR*, pages 2657–2664, 2011. 2, 11, 12, 13, 14, 15, 16, 17, 18, 19

[14] J. Pan, Z. Hu, Z. Su, and M.-H. Yang. Deblurring face images with exemplars. In *ECCV*, pages 47–62, 2014. 23

[15] J. Pan, Z. Hu, Z. Su, and M.-H. Yang. Deblurring text images via L_0-regularized intensity and gradient prior. In *CVPR*, pages 2901–2908, 2014. 11, 12, 14, 15, 16, 17, 19, 22

[16] Q. Shan, J. Jia, and A. Agarwala. High-quality motion deblurring from a single image. In *SIGGRAPH*, 2008. 2, 10, 14, 19

[17] L. Sun, S. Cho, J. Wang, and J. Hays. Edge-based blur kernel estimation using patch priors. In *ICCP*, 2013. 5, 9

[18] O. Whyte, J. Sivic, and A. Zisserman. Deblurring shaken and partially saturated images. In *ICCV Workshops*, pages 745–752, 2011. 1, 4, 11

[19] O. Whyte, J. Sivic, A. Zisserman, and J. Ponce. Non-uniform deblurring for shaken images. *IJCV*, 98(2):168–186, 2012. 10, 11, 23

[20] L. Xu and J. Jia. Two-phase kernel estimation for robust motion deblurring. In *ECCV*, pages 157–170, 2010. 2, 4, 14, 15, 16, 17, 18, 19, 20, 21

[21] L. Xu, S. Zheng, and J. Jia. Unnatural L_0 sparse representation for natural image deblurring. In *CVPR*, pages 1107–1114, 2013. 2, 4, 5, 6, 10, 11, 12, 13, 14, 15, 16, 17, 18, 19, 20, 21

[22] L. Zhong, S. Cho, D. Metaxas, S. Paris, and J. Wang. Handling noise in single image deblurring using directional filters. In *CVPR*, pages 612–619, 2013. 5, 8, 11, 13, 14, 16, 17, 22